Large Intelligent Surface-Assisted Nonorthogonal Multiple Access for 6G Networks: Performance Analysis

Lina Bariah, *Member, IEEE*, Sami Muhaidat, *Senior Member, IEEE*, Paschalis C. Sofotasios, *Senior Member, IEEE*, Faissal El Bouanani, *Senior Member, IEEE*, Octavia A. Dobre, *Fellow, IEEE*, and Walaa Hamouda, *Senior Member, IEEE*

***Abstract*—Large intelligent surface (LIS) has recently emerged as a potential enabling technology for 6G networks, offering extended coverage and enhanced energy and spectral efficiency. In this work, motivated by its promising potentials, we investigate the error rate performance of LIS-assisted nonorthogonal multiple access (NOMA) networks. Specifically, we consider a downlink NOMA system, in which data transmission between a base station (BS) and L NOMA users is assisted by an LIS comprising M reflective elements (REs). First, we derive the probability density function (PDF) of the end-to-end wireless fading channels between the BS and NOMA users. Then, by leveraging the obtained results, we derive an approximate expression for the pairwise error probability (PEP) of NOMA users under the assumption of imperfect successive interference cancellation. Furthermore, accurate expressions for the PEP for $M = 1$ and large M values ($M > 10$) are presented in closed-form. To gain further insights into the system performance, an asymptotic expression for PEP in high signal-to-noise ratio regime, asymptotic diversity order, and tight union bound on the bit error rate are provided. Finally, numerical and simulation results are presented to validate the derived mathematical results.**

***Index Terms*—6G, asymptotic diversity order, bit error rate (BER), large intelligent surfaces (LISs), nonorthogonal multiple access (NOMA), pairwise error probability (PEP), union bound.**

Manuscript received August 5, 2020; revised October 18, 2020 and December 1, 2020; accepted January 26, 2021. Date of publication February 5, 2021; date of current version March 24, 2021. This work was supported in part by Khalifa University under Grant EX2020-037-8434000382 and Grant EX2020-038-8434000383. The work of Octavia A. Dobre was supported in part by the Natural Sciences and Engineering Research Council of Canada, through its Discovery program. *(Corresponding author: Sami Muhaidat.)*

Lina Bariah is with the KU Center for Cyber-Physical Systems, Department of Electrical and Computer Engineering, Khalifa University, Abu Dhabi, UAE (e-mail: lina.bariah@ieee.org).

Sami Muhaidat are with the KU Center for Cyber-Physical Systems, Department of Electrical and Computer Engineering, Khalifa University, Abu Dhabi, UAE, and the Department of Systems and Computer Engineering, Carleton University, Ottawa, ON K1S 5B6, Canada.(e-mail: muhaidat@ieee.org).

Paschalis C. Sofotasios is with the Center for Cyber-Physical Systems, Department of Electrical and Computer Engineering, Khalifa University, Abu Dhabi, UAE, and also with the Department of Electrical Engineering, Tampere University, 33101 Tampere, Finland (e-mail: p.sofotasios@ieee.org).

Faissal El Bouanani is with the ENSIAS College of Engineering, Mohammed V University, Rabat 10000, Morocco (e-mail: f.elbouanani@um5s.net.ma).

Octavia A. Dobre is with the Department of Electrical and Computer Engineering, Memorial University, St. John's, NL A1B 3X5, Canada (e-mail: odobre@mun.ca).

Walaa Hamouda is with the Department of Electrical and Computer Engineering, Concordia University, Montreal, QC H3G 1M8, Canada (e-mail: hamouda@ece.concordia.ca).

Digital Object Identifier 10.1109/JIOT.2021.3057416

I. Introduction

THE ONGOING deployment of the fifth-generation (5G) mobile networks aims to realize the vision of "connected everything," enabling distinguished paradigms of wireless communications, including machine-to-people communications, machine-to-machine communications, and people-to-people communications [1]. These new paradigms are expected to connect a massive number of heterogeneous data-hungry devices with diverse requirements, resulting in a spectrum shortage crisis, in addition to degraded latency and increased energy consumption. This stimulates the call for the development of innovative technologies, which are capable of supporting massive connectivity, extremely high data rates, and ultra-low latency.

A promising technology, i.e., nonorthogonal multiple access (NOMA), has emerged as a key enabling technology for 5G networks, which offers reduced latency, enhanced connectivity and reliability, and improved energy and spectral efficiency [2], [3]. Two NOMA categories were proposed in the literature, namely, power-domain NOMA (PD-NOMA) and code-domain NOMA (CD-NOMA). The principle concept of downlink PD-NOMA is to employ superposition coding at the base station (BS) by sorting out users based on their channel gains, and then, multiplex their signals in power domain [4], [5]. Interference mitigation in PD-NOMA is carried out by performing successive interference cancellation (SIC) for users' signals with higher power levels [6]. On the other hand, users' signals with low-power levels are treated as noise. To realize efficient SIC, and hence, efficient NOMA system, paired users should have distinct channel conditions [7]. Alternatively, in CD-NOMA, different users are assigned different sparse codewords and then multiplexed simultaneously over the same frequency resources. At the users' end, a message passing algorithm (MPA)-based receiver is used to enable multiuser detection (MUD). Although CD-NOMA can provide enhanced performance, the high complexity of the codebook designs and MPA-based receivers represents a major challenge in such systems. More precisely, users' codebooks should be known at the receiver side in order to realize MUD. It was shown that MPA-based receivers usually have higher complexity than SIC-based receivers [8]. Therefore, in the current work, PD-NOMA is considered and the term NOMA refers to PD-NOMA in the rest of this article.

Due to the highly stochastic nature of the wireless channels, wireless incident signals are susceptible to several impairments, such as random fluctuation, path loss, blockage, and absorption, yielding uncontrollable multipath fading environments. Such impairments can be overcome by employing multiple-input–multiple-output schemes. However, this comes at the expense of reduced energy efficiency, which constitutes a fundamental challenge in the 5G and beyond wireless networks [9]. Large intelligent surface (LIS) has recently emerged as a disruptive energy and spectrally efficient technology, which is capable of offering a programmable control over the wireless environment [10], [11]. This can be realized by incorporating reflective elements (REs) that manipulate the impinging electromagnetic waves to perform various functionalities, such as wave reflection, refraction, absorption, steering, focusing, and polarization [12]. In light of this, extensive research efforts have been made toward characterizing the unique properties of LISs, in addition to proposing enhancing schemes and investigating their performance in different scenarios, e.g., [13]–[20].

In the context of NOMA, it was shown that LIS can tune the propagation environment to guarantee specific users' order, and hence, enabling efficient deployment of NOMA systems. Furthermore, by efficiently utilizing LIS, it becomes more feasible to change users' order to satisfy a particular system requirement according to certain users priorities, rather than relying on the random propagation environment of wireless systems. Therefore, motivated by the envisioned potentials of LIS, the integration of LIS into NOMA systems has recently received an increasing attention from the research community [21]–[26].

A. LIS-Enabled NOMA in Massive IoT Networks

In massive power-constrained Internet-of-Things (IoT) networks, the enhanced energy and spectral efficiency can be achieved by limiting the communication range to short distances. In this respect, LIS is considered as a promising energy-efficient solution to extend the communication range [27]. Multiple LISs can be efficiently utilized in order to connect far IoT devices, and to allow these devices to reliably communicate with higher data rates. This can be accomplished at LISs by altering the properties of the multiple beams reflected from the REs, to enable constructive combining of these beams, and hence, increase the received signals' qualities.

Apart from the extended communication range, LIS offers additional advantages to massive IoT networks.

1) Physical layer security can be enhanced in IoT devices by destructively combining the reflected beams from the LIS to prevent signals' leakage to illegal devices [28].
2) Wireless power transfer in massive IoT networks is a prominent application for LIS. Specifically, multiple LISs can be exploited to provide additional transmission links for energy harvesting purposes, where it was shown that LIS links assist in enhancing the harvested power in energy-limited IoT devices [29].

On the other hand, although NOMA has been widely considered as an energy and spectrally efficient solution to support massive connectivity in massive IoT networks [30], ensuring channels ordering, and hence, particular resource and power allocation schemes, is considered as a key challenge in such networks. In particular, as the number of devices increases, it is more likely that some users will experience identical channel gains, yielding unreliable multiuser detection, and hence, severe performance degradation [31]. Within this context, the use of LISs can help to overcome this limitation by smartly tuning the wireless environment to guarantee specific channels ordering [9].

B. Related Work

The existing research works have primarily focused on investigating the performance of LIS-assisted NOMA systems, in addition to proposing enhancement schemes to optimize the performance of these systems in terms of outage probability and achievable rate. Fu *et al.* [26] formulated a joint optimization problem to obtain optimum beamforming vector and phase-shift matrix at the LIS that minimize the total transmission power of a downlink NOMA system. It was demonstrated that LIS can potentially reduce the total transmission power in NOMA systems. Li *et al.* [32] considered an LIS-assisted multicluster multiple-input single-output (MISO) NOMA system. They proposed a mathematical framework in order to jointly optimize the beamforming vector at BS and the reflection coefficient vector at LIS. Yang *et al.* [25] formulated an optimization problem and proposed a solution to maximize users' data rates, while ensuring users' fairness in a downlink LIS-based NOMA system. Transmit beamforming and phase-shift vector optimization have been investigated in the literature under different scenarios and for various setups [21], [22], [24], [33]–[35]. Hou *et al.* [36] analyzed outage probability, ergodic rate, diversity order, and spectral and energy efficiencies of users with higher priority in an LIS-assisted NOMA scenario while considering direct links between the BS and NOMA users. The reported results in [36] demonstrated that the effect of the direct link is negligible, especially for a large number of REs. Yue and Liu [37] investigated the effect of residual interference due to imperfect SIC on the outage probability and ergodic rate performance of LIS-based NOMA systems. The reported results in [37] highlighted the advantages of incorporating NOMA with LIS, compared to OMA, to enhance the outage probability and ergodic rate performance.

While the performance of LIS-assisted NOMA systems has been analyzed in the literature, a comprehensive error rate analysis is still missing, although it is the most revealing metric about the system performance. The error rate performance of an LIS-based NOMA system was addressed in [38] for the special case of two users. Thirumavalavan and Jayaraman [38] derived two bit error rate (BER) expressions for the two users under specific modulation schemes. Moreover, the central limit

theorem (CLT) was adopted in [38], limiting the analytical framework to a large number of REs.

C. Contribution

Motivated by the above discussion, in this article, we provide a comprehensive analytical framework to investigate the error rate performance of an LIS-based NOMA system. The proposed work is valid for an arbitrary modulation scheme and any number of users. The main contributions of this article are summarized as follows.

1) We derive a tight approximate PDF expression for the end-to-end (e2e) wireless channel of the underlying downlink LIS-based NOMA system, with L users and M REs.
2) We derive a novel pairwise error probability (PEP) expression of NOMA users, under the assumption of imperfect SIC. The derived PEP expression is then utilized to obtain a union bound on the error rate.
3) We derive PEP expressions for the special cases of $M = 1$ and large M ($M > 10$), where the latter is obtained by utilizing the CLT.
4) We further analyze the asymptotic PEP for general M values. The derived asymptotic PEP is then used to investigate the asymptotic diversity order and quantify the effect of the number of REs on the error rate performance of NOMA users.

The remainder of this article is organized as follows. Section II introduces the system model of a downlink LIS-based NOMA system. An accurate PEP analysis for an arbitrary number of REs (M) is presented in Section III, while the asymptotic PEP analysis and the asymptotic diversity order are investigated in Section IV. Numerical and simulation results are presented in Section V and this article is concluded in Section VI.

Notations: The complex conjugate operation and the absolute value are denoted as $(\cdot)^*$ and $|.|$, respectively. $\Re\{.\}$ represents the real part of a complex number, $\hat{x}$ is a detected symbol, while $\bar{x}$ denotes an erroneously detected symbol. The expectation operator is denoted as $\mathbb{E}(.)$. $\mathcal{CN}(\mu, \sigma^2)$ represents the circularly symmetric complex Gaussian (CSCG) distribution with mean μ and variance σ^2.

II. System Model

In this work, we consider a downlink LIS-assisted NOMA system comprising a single LIS with $\bar{M}$ REs to assist in data transmission between a single BS and L NOMA users, $U_1, \ldots, U_L$. It is further assumed that the LIS is divided into L zones, $Z_1, \ldots, Z_L$, each comprising M REs, $M = \bar{M}/L$. Furthermore, the lth zone is responsible for reflecting the signal toward the lth user, as depicted in Fig. 1. Following the principle of NOMA, the BS broadcasts a superposed message that consists of L messages intended for the L users, multiplexed in power domain. Without loss of generality, we assume that the large-scale fading is dominant, and hence, channel qualities are determined based on the users' distances from the LIS. Subsequently, we consider that the first user U_1 is the farthest user from the LIS, i.e., the user with the weakest link. On the other hand, the Lth user U_L is the nearest user to the LIS, and, therefore, it experiences the strongest channel, i.e., $d_{R,1} > \cdots > d_{R,L}$, where $d_{R,l}$ represents the distance from the LIS to the lth user. The power coefficients are allocated to the users based on their locations, in which far users are allocated higher power levels than near users. It is worth highlighting that our analytical framework is valid for both near-field and far-field scenarios. For the sake of simplicity, in this work, we consider the far-field scenario. In particular, we assume that the distances between the REs in the lth zone and the lth user are identical. Note that for near-field scenarios, the distances between the REs should be taken into consideration [39].

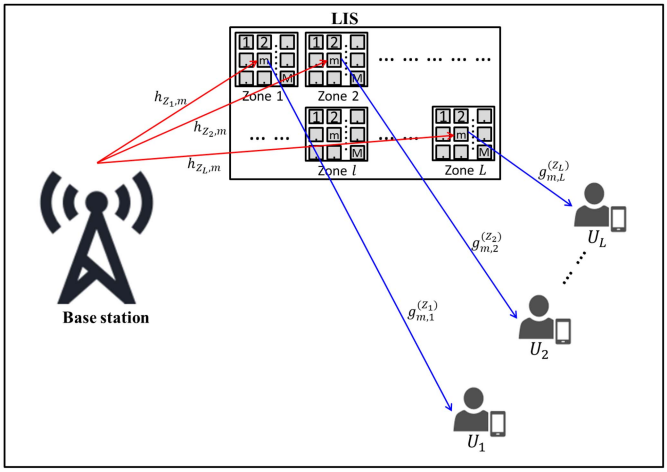

Fig. 1. LIS-based NOMA system model with L users.

The baseband received signal at the lth user can be written as

$$r_l = \frac{1}{\sqrt{d_B^{\alpha} d_{R,l}^{\alpha}}} \sum_{m=1}^{M} h_{Z_l,m} g_{m,l}^{(Z_l)} w_{Z_l,m} e^{j\theta_{m,l}} \sum_{i=1}^{L} \sqrt{P_i}\, x_i + n_l \quad (1)$$

where $h_{Z_l,m}$ represents the small-scale fading channel between the BS and the mth RE in the lth zone, while $g_{m,l}^{(Z_l)}$ represents the fading channel between the mth RE in the lth zone and the lth user. For the sake of simplicity, in the rest of this article, we will drop the zone index from $h_{Z_l,m}$ and $g_{m,l}^{(Z_l)}$, i.e., h_m and $g_{m,l}$ will denote $h_{Z_l,m}$ and $g_{m,l}^{(Z_l)}$, respectively. Assuming that the line-of-sight (LoS) components in the BS-LIS and LIS-lth user ($\forall l$) links are unavailable, both h_m and $g_{m,l}$ are CSCG distributed with zero mean and variance σ^2. Additionally, $w_{Z_l,m}$ represents the amplitude reflection coefficient, which is assumed to be normalized to unity [24], while $\theta_{m,l}$ is the phase shift applied by the mth RE in the the lth zone. Moreover, x_i and P_i are the transmitted symbol and the power level of the ith user, respectively, and α accounts for the path-loss exponent. For simplicity, the total transmission power of the BS is normalized to unity, i.e., $P_T = 1$. Hence, the transmit power dedicated to the ith message equals to the power coefficient allocated to the ith user, $P_i = \rho_i P_T = \rho_i$, where ρ_i is the ith power coefficient. Note that the distance between the BS and LIS is denoted by d_B. The additive white Gaussian noise

(AWGN) is represented by $n_l \sim \mathcal{CN}(0, N_0)$, where N_0 stands for the noise power spectral density.

Assuming perfect knowledge of the channels phases, θ_{h_m} and $\theta_{g_{m,l}}$ of h_m and $g_{m,l}$, respectively, the phase shift of the mth RE is chosen as $\theta_{m,l} = -(\theta_{h_m} + \theta_{g_{m,l}})$. Subsequently, the received signal at the lth user can be rewritten as

$$r_l = q_l \sum_{i=1}^{L} \sqrt{P_i}\, x_i + n_l \tag{2}$$

where q_l denotes the e2e channel coefficient, which is given by

$$q_l = \frac{1}{\sqrt{d_B^{\alpha} d_{R,l}^{\alpha}}} \sum_{m=1}^{M} |h_m| \big| g_{m,l} \big|. \tag{3}$$

Multiuser interference at the lth user is canceled by employing SIC for higher power signals, i.e., $x_1, \ldots, x_{l-1}$, whereas the lower power users' signals, i.e., $x_{l+1}, \ldots, x_L$, are treated as additive noise. Hence, the output signal of the lth SIC receiver can be written as

$$r_l' = q_l \Big(\sqrt{P_l}\, x_l + X_l \Big) + n_l \tag{4}$$

with

$$X_l = \sum_{i=1}^{l-1} \sqrt{P_i}\, \delta_i + \sum_{j=l+1}^{L} \sqrt{P_j}\, x_j \tag{5}$$

where $\delta_i = x_i - \hat{x}_i$ denotes the output of the ith SIC iteration and $\hat{x}_i$ denotes the corresponding detected symbol. Note that δ_i has two scenarios, namely, $\delta_i = 0$ and $\delta_i \neq 0$ for successful and unsuccessful SIC, respectively.

III. Pairwise Error Probability Analysis

In this section, we derive an accurate expression for the PEP, which offers useful insights into the error rate performance of the considered scenario. In particular, the PEP quantifies the error probability under specific scenario of transmitted and detected symbols. Moreover, the derivation of the PEP constitutes the basic block for obtaining an upper bound on the BER. The PEP of the lth user is defined as the probability of erroneously decoding symbol $\bar{x}_l$ given that symbol x_l was transmitted, where $\bar{x}_l \neq x_l$,$\forall l$. Therefore, based on the maximum-likelihood (ML) rule, the conditional PEP of the lth user can be expressed as

$$\Pr(x_l \to \bar{x}_l \mid q_l) = \Pr\Big(\Big| r_l' - q_l \sqrt{P_l} \bar{x}_l \Big|^2 \leq \Big| r_l' - q_l \sqrt{P_l} x_l \Big|^2 \Big). \tag{6}$$

Note that the PEP expression in (6) is conditioned on the fading coefficient q_l and on transmitted and detected symbols of all users. By inserting (4) into (6), and after some mathematical simplifications, the PEP can be rewritten as

$$\Pr(x_l \to \bar{x}_l \mid q_l) = \Pr\Big(\Big| q_l (\sqrt{P_l} \bar{\Delta}_l + X_l) + n_l \Big|^2 \leq |q_l X_l + n_l|^2 \Big) \tag{7}$$

where $\bar{\Delta}_l = x_l - \bar{x}_l$.

After expanding (7), the conditional PEP can be expressed as in (8), shown at the bottom of the page. Conditioned on q_l, the noise term N_l in (8) is modeled as a Gaussian random variable (RV) with zero mean and variance $\sigma_N^2 = 2P_l |\bar{\Delta}_l|^2 N_0$. Hence, the conditional PEP can be evaluated as

$$\Pr(x_l \to \bar{x}_l \mid q_l = q) = Q\Big(\frac{q \vartheta_l}{\lambda_l} \Big) \tag{9}$$

where $Q(\cdot)$ represents the Gaussian Q-function. Also

$$\vartheta_l = \sqrt{P_l} \big| \bar{\Delta}_l \big|^2 + 2\Re\big\{ \bar{\Delta}_l X_l^* \big\} \tag{10}$$

and

$$\lambda_l = \big| \bar{\Delta}_l \big| \sqrt{2N_0}. \tag{11}$$

By applying the Chernoff bound on the Q-function in (9), the conditional PEP can be bounded by [40]

$$\Pr(x_l \to \bar{x}_l \mid q_l = q) \leq \exp\Big(-\frac{q^2 \vartheta_l^2}{2\lambda_l^2} \Big). \tag{12}$$

To obtain the unconditional PEP, we average over the PDF of the total fading coefficient, q_l, where $q_l \geq 0$.

Proposition 1: The PDF of q_l can be approximated by

$$f_{q_l}(q) \approx a_1 \sqrt{d_B^{\alpha} d_{R,l}^{\alpha}}\, G_{1,2}^{2,0}\left(\frac{\sqrt{d_B^{\alpha} d_{R,l}^{\alpha}}\, q}{a_2} \middle| \begin{matrix} -; a_3 \\ a_4, a_5; - \end{matrix} \right) \tag{13}$$

where $G_{p,q}^{m,n}(. \mid .)$ denotes the standard Meijer's G-function

$$a_1 = \frac{\Gamma(a_3 + 1)}{a_2 \Gamma(a_4 + 1) \Gamma(a_5 + 1)} \tag{14}$$

$$a_2 = \frac{a_3}{2}(\varphi_4 - 2\varphi_3 + \varphi_2) + 2\varphi_4 - 3\varphi_3 + \varphi_2 \tag{15}$$

$$a_3 = \frac{4\varphi_4 - 9\varphi_3 + 6\varphi_2 - \mu_1}{-\varphi_4 + 3\varphi_3 - 3\varphi_2 + \mu_1} \tag{16}$$

$$a_4 = \frac{a_6 + a_7}{2} \tag{17}$$

$$a_5 = \frac{a_6 - a_7}{2} \tag{18}$$

$$a_6 = \frac{a_3(\varphi_2 - \mu_1) + 2\varphi_2 - \mu_1}{a_2} - 3 \tag{19}$$

$$a_7 = \sqrt{\left(\frac{a_3(\varphi_2 - \mu_1) + 2\varphi_2 - \mu_1}{a_2} - 1 \right)^2 - 4\frac{\mu_1(a_3 + 1)}{a_2}} \tag{20}$$

and

$$\varphi_i = \frac{\mu_i}{\mu_{i-1}}, \quad i \geq 1 \tag{21}$$

$$\Pr(x_l \to \bar{x}_l \mid q_l) = \Pr\left(\underbrace{2\sqrt{P_l}\Re\big\{ \bar{\Delta}_l n_l^* \big\}}_{N_l} \leq -q_l \Big(\Big| \sqrt{P_l} \bar{\Delta}_l + X_l \Big|^2 - |X_l|^2 \Big) \right) \tag{8}$$

where $\Gamma(\cdot)$ represents the complete Gamma function [41], and μ_i is the ith moment of q_l and $\mu_0 = 1$. The first four moments of q_l are given by

$$\mu_1 = \frac{M\pi\sigma^2}{2} \tag{22}$$

$$\mu_2 = \left(4 + (M-1)\frac{\pi^2}{4}\right)M\sigma^4 \tag{23}$$

and, μ_3 and μ_4 are given in (24) and (25), respectively, shown at the bottom of the page.

Proof: The derivation of PDF and the corresponding moments is provided in the Appendix. ∎

Therefore, using the derived PDF jointly with (12), the unconditional PEP can be tightly approximated as

$$\Pr(x_l \to \bar{x}_l) \approx a_1\sqrt{d_B^\alpha d_{R,l}^\alpha}\int_0^\infty \exp\left(-\frac{q^2\vartheta_l^2}{2\lambda_l^2}\right) \times G_{1,2}^{2,0}\left(\frac{\sqrt{d_B^\alpha d_{R,l}^\alpha}q}{a_2}\middle| \begin{matrix} -; a_3 \\ a_4, a_5; - \end{matrix}\right) dq. \tag{26}$$

Utilizing the following Meijer's G-function representation of the exponential function [42, eq. (8.4.3.1)]

$$\exp(-z) = G_{0,1}^{1,0}\left(z\middle| \begin{matrix} -; - \\ 0; - \end{matrix}\right) \tag{27}$$

the integral in (26) can be rewritten as follows:

$$\Pr(x_l \to \bar{x}_l) \approx a_1\sqrt{d_B^\alpha d_{R,l}^\alpha}\int_0^\infty G_{0,1}^{1,0}\left(\frac{q^2\vartheta_l^2}{2\lambda_l^2}\middle| \begin{matrix} -; - \\ 0; - \end{matrix}\right) \times G_{1,2}^{2,0}\left(\frac{\sqrt{d_B^\alpha d_{R,l}^\alpha}q}{a_2}\middle| \begin{matrix} -; a_3 \\ a_4, a_5; - \end{matrix}\right) dq. \tag{28}$$

The integral in (28) can be solved using [42, eq. (2.24.1.1)]. Hence, the unconditional PEP can be evaluated as

$$\Pr(x_l \to \bar{x}_l) \approx \frac{a_1 a_2 2^{a_4+a_5-a_3}}{\sqrt{\pi}} \times G_{4,3}^{1,4}\left(\zeta_l\middle| \begin{matrix} \frac{-a_4}{2}, \frac{1-a_4}{2}, \frac{-a_5}{2}, \frac{1-a_5}{2}; - \\ 0; \frac{-a_3}{2}, \frac{1-a_3}{2} \end{matrix}\right) \tag{29}$$

where

$$\zeta_l = \frac{2a_2^2\vartheta_l^2}{d_B^\alpha d_{R,l}^\alpha \lambda_l^2}. \tag{30}$$

In the following, to obtain insights into the system performance, we consider the following two special cases, in which the corresponding PEP expressions are derived.

Case 1 ($M = 1$): For $M = 1$, the PEP of the lth user can be upper bounded by

$$\Pr(x_l \to \bar{x}_l) \le \eta_l \exp(\eta_l) E_1(\eta_l) \tag{31}$$

where $E_1(z) = \int_z^\infty (e^{-t}/t)\,dt$ represents the exponential integral function, and

$$\eta_l = \frac{\lambda_l^2 d_B^\alpha d_{R,l}^\alpha}{2\sigma^4\vartheta_l^2}. \tag{32}$$

Proof: For the special case of $M = 1$, the fading coefficient q_l reduces to

$$(q_l)_{M=1} \to \grave{q}_l = \frac{|h_1||g_{1,l}|}{\sqrt{d_B^\alpha d_{R,l}^\alpha}} \tag{33}$$

which is a double Rayleigh RV with PDF given by [43]

$$f_{\grave{q}_l}(q) = \frac{q\sqrt{d_B^\alpha d_{R,l}^\alpha}}{\sigma^4} K_0\left(\frac{q\sqrt{d_B^\alpha d_{R,l}^\alpha}}{\sigma^2}\right) \tag{34}$$

where $K_0(\cdot)$ represents the zero-order modified Bessel function of the second kind. Subsequently, using (12) and (34), the unconditional PEP for $M = 1$ can be evaluated as follows:

$$\Pr(x_l \to \bar{x}_l) \le \frac{\sqrt{d_B^\alpha d_{R,l}^\alpha}}{\sigma^4}\int_0^\infty q\exp\left(-\frac{q^2\vartheta_l^2}{2\lambda_l^2}\right) \times K_0\left(\frac{q\sqrt{d_B^\alpha d_{R,l}^\alpha}}{\sigma^2}\right) dq. \tag{35}$$

Finally, the integral in (35) can be solved using [44, eq. (2.16.8.6)], yielding (31). ∎

Case 2 ($M > 10$): For a sufficiently large number of REs, the PEP of the lth user can be evaluated as

$$\Pr(x_l \to \bar{x}_l) \approx \sqrt{\frac{d_B^\alpha d_{R,l}^\alpha}{8\xi_l\bar{\sigma}_l^2}}\exp\left(\frac{d_B^\alpha d_{R,l}^\alpha \bar{\mu}_l^2}{4\xi_l\bar{\sigma}_l^4} - \frac{\bar{\mu}_l^2}{2\bar{\sigma}_l^2}\right) \times \left[1 + \operatorname{erf}\left(\sqrt{\frac{d_B^\alpha d_{R,l}^\alpha \bar{\mu}_l^2}{4\xi_l\bar{\sigma}_l^4}}\right)\right] \tag{36}$$

where

$$\xi_l = \frac{\vartheta_l^2\bar{\sigma}_l^2 + d_B^\alpha d_{R,l}^\alpha \lambda_l^2}{2\bar{\sigma}_l^2\lambda_l^2} \tag{37}$$

$$\mu_3 = \begin{cases} M\pi\left(\frac{9}{2} + 6(M-1) + (M-1)(M-2)\frac{\pi^2}{8}\right)\sigma^6, M \ge 3 \\ 21\pi\sigma^6, M = 2 \\ \frac{9\pi\sigma^6}{2}, M = 1 \end{cases} \tag{24}$$

$$\mu_4 = \begin{cases} \left(64M + 48M(M-1) + 9M(M-1)\pi^2 + 6M(M-1)(M-2)\pi^2 + \frac{M(M-1)(M-2)(M-3)\pi^4}{16}\right)\sigma^8, M \ge 4 \\ \left(480 + 90\pi^2\right)\sigma^8, M = 3 \\ \left(224 + 18\pi^2\right)\sigma^8, M = 2 \\ 64\sigma^8, M = 1 \end{cases} \tag{25}$$

$$\bar{\mu}_l = \frac{M\pi\sigma^2}{2} \tag{38}$$

$$\bar{\sigma}_l^2 = \frac{M\sigma^2\left(16-\pi^2\right)}{4} \tag{39}$$

and erf$(\cdot)$ denotes the error function.

Proof: For a sufficiently large number of REs, $M > 10$, according to the CLT [45], the e2e cascaded fading coefficient q_l in (3) reduces to a normally distributed RV, $(q_l)_{M>10} \rightarrow \tilde{q}_l \sim \mathcal{N}(\bar{\mu}_l, \bar{\sigma}_l)$ with mean and variance obtained from (38) and (39), respectively.

Hence, the PDF of $\tilde{q}_l$ can be expressed as the following:

$$f_{\tilde{q}_l}(q) = \frac{1}{\sqrt{2\pi\bar{\sigma}_l^2}} \exp\left(-\frac{(q-\bar{\mu}_l)^2}{2\bar{\sigma}_l^2}\right). \tag{40}$$

Accordingly, for the case of a large number of REs, the PEP can be evaluated by averaging (12) over $\tilde{q}$, which has the PDF given by (40). After some mathematical manipulations, the unconditional PEP can be written as follows:

$$\Pr(x_l \rightarrow \bar{x}_l) \approx \frac{\exp\left(-\frac{\bar{\mu}_l^2}{2\bar{\sigma}_l^2}\right)}{\sqrt{2\pi\bar{\sigma}_l^2}} \times \int_0^\infty \exp\left(-\frac{q^2\left(\vartheta_l^2\bar{\sigma}_l^2+\lambda_l^2\right)}{2\bar{\sigma}_l^2\lambda_l^2} + \frac{\bar{\mu}_l q}{\bar{\sigma}_l^2}\right) dq. \tag{41}$$

The integral in (41) can be evaluated using [41, eq. (3.322.2)]. That is, (36) is obtained, which concludes the proof. ∎

A. Union Bound on the BER Performance

The derived PEP in (29) is leveraged to compute an accurate upper bound on the average error probability of NOMA users. Note that the BER union bound is defined as the weighted sum of all PEP values, considering all transmitted and detected symbols scenarios for all users, including perfect and imperfect SIC [46]. Hence, utilizing the derived PEP expression in (29), the BER union bound can be written as [47, eq. (4.2–70)]

$$P_e = \frac{1}{\tau}\sum_{x_l}\sum_{\substack{\bar{x}_l \\ \bar{x}_l \neq x_l}} \Pr(x_l \rightarrow \bar{x}_l) \tag{42}$$

where τ denotes the number of possible combinations of x_l and $\bar{x}_l$ $\forall l$.

IV. Asymptotic Diversity Order

The PEP has been widely adopted as an efficient metric to quantify the asymptotic diversity order, which is defined as the slope of the PEP at high signal-to-noise ratio (SNR) regime. The asymptotic diversity order of the lth user can be evaluated as

$$d_s = -\lim_{\bar{\gamma}\rightarrow\infty} \frac{\log(\Pr(x_l \rightarrow \bar{x}_l))}{\log\bar{\gamma}} \tag{43}$$

where $\bar{\gamma}$ is the average transmit SNR of the lth user. To obtain the asymptotic diversity order, we first exploit the asymptotic expansion of Meijer's G-function from [48, eq. (41)] to approximate (29) when $\bar{\gamma} \rightarrow \infty$. Note that as $\bar{\gamma} \rightarrow \infty$, the argument of Meijer's G-function in (29) approaches infinity. Therefore, utilizing the asymptotic expansion of Meijer's G-function in [48, eq. (41)], the PEP of the lth user can be asymptotically given as

$$\begin{aligned}\Pr(x_l \rightarrow \bar{x}_l) \sim\ & a_1 a_2 2^{a_4+a_5-a_3} \times \Bigg[-\zeta_l^{-\left(\frac{a_4}{2}+1\right)} \frac{2\Gamma\left(-\frac{a_4-a_5}{2}\right)\Gamma\left(-\frac{a_4-a_5+1}{2}\right)\Gamma\left(1+\frac{a_4}{2}\right)}{\Gamma\left(-\frac{a_4-a_3}{2}\right)\Gamma\left(-\frac{a_4-a_3+1}{2}\right)} \\ & + \zeta_l^{-\left(\frac{a_4}{2}+\frac{1}{2}\right)} \frac{\Gamma\left(\frac{1-a_4+a_5}{2}\right)\Gamma\left(-\frac{a_4-a_5}{2}\right)\Gamma\left(\frac{1+a_4}{2}\right)}{\Gamma\left(\frac{1-a_4+a_3}{2}\right)\Gamma\left(-\frac{a_4-a_3}{2}\right)} \\ & - \zeta_l^{-\left(\frac{a_5}{2}+1\right)} \frac{2\Gamma\left(-\frac{a_5-a_4}{2}\right)\Gamma\left(-\frac{a_5-a_4+1}{2}\right)\Gamma\left(1+\frac{a_5}{2}\right)}{\Gamma\left(-\frac{a_5-a_3}{2}\right)\Gamma\left(-\frac{a_5-a_3+1}{2}\right)} \\ & + \zeta_l^{-\left(\frac{a_5}{2}+\frac{1}{2}\right)} \frac{\Gamma\left(\frac{1-a_5+a_4}{2}\right)\Gamma\left(-\frac{a_5-a_4}{2}\right)\Gamma\left(\frac{1+a_5}{2}\right)}{\Gamma\left(\frac{1-a_5+a_3}{2}\right)\Gamma\left(-\frac{a_5-a_3}{2}\right)} \Bigg]. \end{aligned} \tag{44}$$

To evaluate the asymptotic diversity order, we substitute (44) in (43) and evaluate the logarithmic function. By considering the dominant components that contribute to the diversity order, the asymptotic diversity order of the lth user can be evaluated as

$$\begin{aligned} d_s &= -\lim_{\bar{\gamma}\rightarrow\infty} \times \left(\frac{\log\left(\bar{\gamma}^{-\left(\frac{a_4}{2}+1\right)} + \bar{\gamma}^{-\left(\frac{a_4}{2}+\frac{1}{2}\right)} + \bar{\gamma}^{-\left(\frac{a_5}{2}+1\right)} + \bar{\gamma}^{-\left(\frac{a_5}{2}+\frac{1}{2}\right)}\right)}{\log(\bar{\gamma})} \right) \\ &= \min\left(\frac{a_4}{2}+\frac{1}{2}, \frac{a_5}{2}+\frac{1}{2}\right) \end{aligned} \tag{45}$$

where a_4 and a_5 are given in (17) and (18), respectively. Fig. 2 shows that $a_5 < a_4$ for all M values. Moreover, it can be noticed from Fig. 2 that a_5 is a function of the number of REs, M; this indicates that the asymptotic diversity order of NOMA users is dependent on the number of REs (M).

V. Numerical and Simulation Results

In this section, we present analytical and Monte Carlo simulation results to corroborate the derived mathematical framework and present insightful conclusions into the performance of LIS-assisted NOMA systems. In particular, we consider a downlink NOMA system with a single BS, a single LIS with M REs, and two users, i.e., $L = 2$. Note that users clustering is used for $L \geq 3$ [49]. Unless mentioned otherwise, we assume that the first user U_1 is the far user located at distance $d_{R,1} = 5$ from the LIS, while the second user U_2 is the near user located at distance $d_{R,2} = 2$ from LIS. Without loss of generality, the distance between the BS and the LIS is normalized to unity, i.e., $d_B = 1$. The power coefficients are allocated as $P_1 = 0.8$ and $P_2 = 0.2$ [2], and the transmitted and detected symbols of all users are selected randomly from

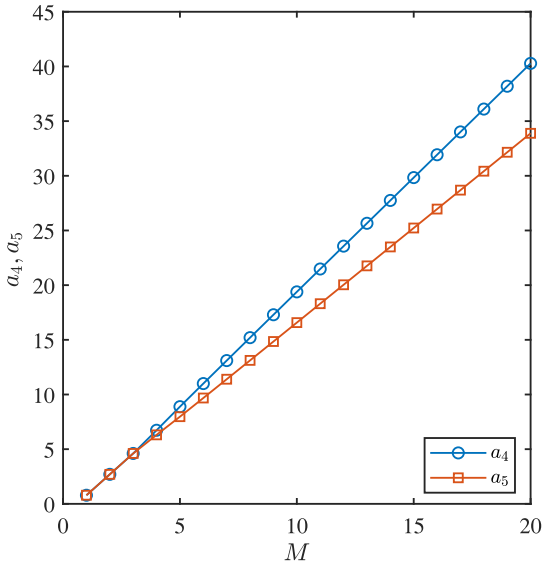

Fig. 2. a_4 and a_5 versus number of REs (M).

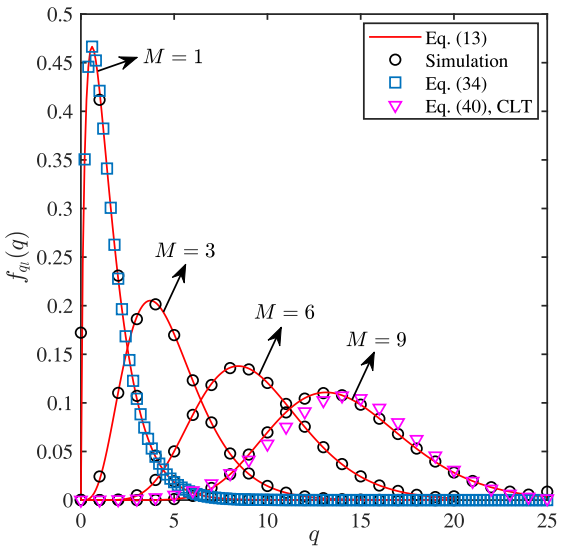

Fig. 3. Analytical and simulated PDF of q_l for different M values.

a binary phase shift keying (BPSK) constellation. Moreover, the path-loss exponent is $\alpha = 3$ [50].

Fig. 3 shows the analytical and simulated PDF of the e2e fading coefficient q_l for $M = 1, 3, 6$, and 9. The results in Fig. 3 confirm the accuracy of the estimated PDF in Proposition 1, and one can observe that the analytical and simulation results perfectly match. Additionally, Fig. 3 corroborates the accuracy of the derived PDF in Proposition 1 for the special cases of $M = 1$ and large M. Specifically, it can be noticed that (13) perfectly matches (34) for $M = 1$. Likewise, for larger values of M, it is observed that (40), derived based on the CLT, closely matches (13). Finally, it is noticed that as M increases, the mean value of q_l increases, resulting in a better average error rate performance. To further confirm the accuracy of (13), the Kullback Leibler (KL) divergence is used to measure the information lost when $f_{q_l}(q)$ is used to approximate $p(q)$. The KL divergence of $f_{q_l}(q)$ from $p(q)$ is

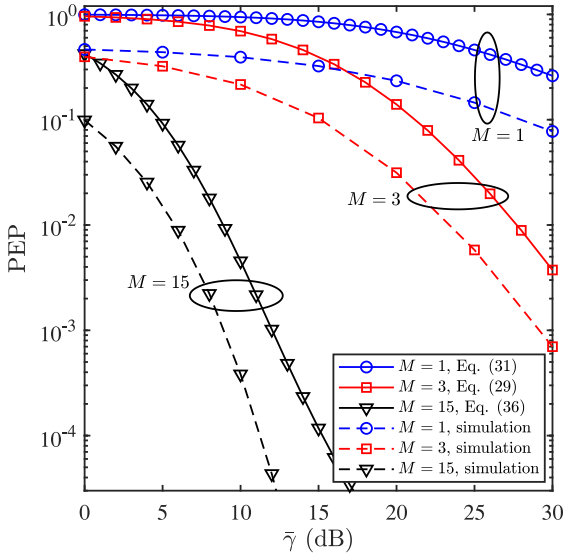

Fig. 4. PEP of the first NOMA user U_1 with different numbers of REs.

TABLE I
KL DIVERGENCE BETWEEN (13) AND MONTE CARLO SIMULATION RESULTS

M	$D_{KL}\left(p\left(q\right) \parallel f_{q_l}(q)\right)$
2	0.009100
3	0.000116
4	0.000341
5	0.000152
6	0.000084
7	0.000052
8	0.000012
9	0.000412

defined as [51]

$$D_{\mathrm{KL}}\big(p(q)\|f_{q_l}(q)\big) = \sum_{q} p(q)\ln\left(\frac{p(q)}{f_{q_l}(q)}\right) \tag{46}$$

where $p(q)$ represents the exact PDF and is obtained via Monte Carlo simulation. Using (46), the evaluation of the KL divergence is shown in Table I. The values represented in Table I corroborates the accuracy of the estimated PDF in Proposition 1.

Fig. 4 depicts the PEP performance of the first user, where the analytical and simulation results are presented for $M = 1, 3$, and 15. Note that the derived bounds/approximants are presented by the solid lines while the exact (simulated) PEP is presented by dashed lines. The simulation results validate the accuracy of the derived expressions in (29), (31), and (36), where it can be observed that the analytical results provide a tight upper bound on the PEP performance over the entire SNR range. Specifically, one can notice that both analytical and simulation results experience the same diversity order, which further confirms the validity of the derived mathematical framework.

The observation in (45) is further validated in Fig. 5, where the asymptotic diversity order of the first user is presented for

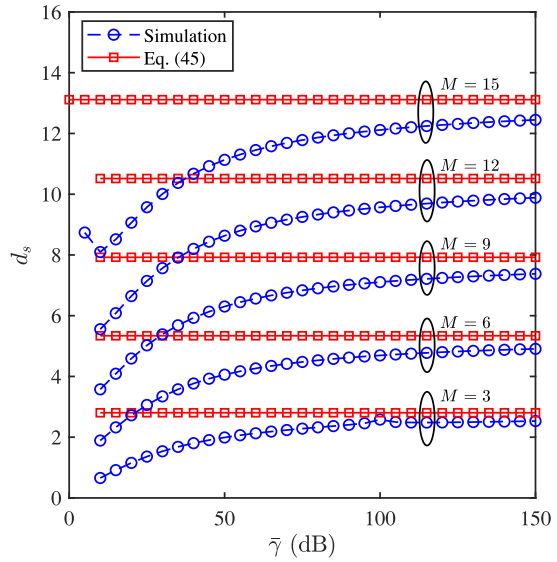

Fig. 5. Asymptotic diversity order of the two users for various values of M.

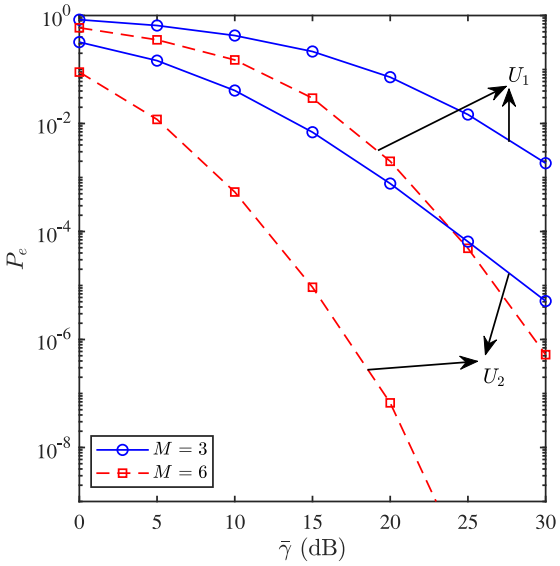

Fig. 6. BER union bound of the two users versus $\bar{\gamma}$ for different numbers of REs.

$M = 3, 6, 9, 12$, and 15. For the sake of clarity, the results of the second user are omitted from Fig. 5, as they are identical to those of the first user. The results in Fig. 5 show that the asymptotic diversity order in the LIS-based NOMA system converges to $(a_5/2) + (1/2)$, where a_5 is a function of M, as depicted in Fig. 2. This observation is verified by Monte Carlo simulations. Fig. 5 highlights the prominent potential of LIS in offering notable enhancement into the error rate performance of NOMA systems, as it is observed that the asymptotic diversity order of the underlying system model is primarily dependent on the number of REs, M.

The BER union bound of the underlying LIS-assisted NOMA system with two users scenario is shown in Fig. 6, for $M = 3$ and $M = 6$. The results confirm the advantages of utilizing LIS to enhance the error rate performance of NOMA. Specifically, in addition to the extended coverage,

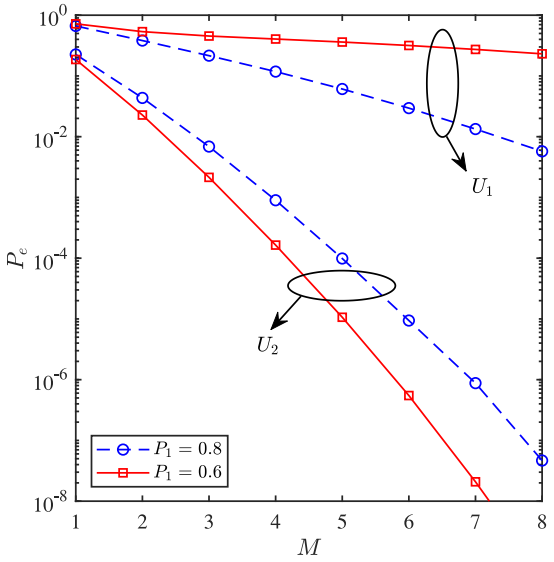

Fig. 7. BER union bound of the two users versus M for different power allocation coefficients, and $\bar{\gamma} = 15$ dB.

the remarkably enhanced error rate performance can be a key driver behind the integration of LIS into NOMA systems. For example, it can observed from Fig. 6 that as M changes from 3 to 6, the performances of the first and second users are enhanced by approximately 9.8 and 10 dB, respectively, at $P_e \approx 1.8 \times 10^{-3}$. Moreover, it can be noticed from Fig. 6 that both users experience the same diversity order.

The effect of the power coefficients and the number of REs is further investigated in Fig. 7, where the BER union bound versus M is presented for $P_1 = 0.8$ and 0.6, at $\bar{\gamma} = 15$ dB. Note that $P_1 > P_2$ and $P_1 + P_2 = 1$. It can be noticed from Fig. 7 that the first user is more susceptible to changes in the power allocation, over different M values. This stems from the fact that the first user does not perform SIC, and hence, changes in the power allocation result in variations in the interference level caused by the second user.

VI. Conclusion

In this article, we proposed a comprehensive mathematical framework to investigate the error rate performance of an LIS-assisted NOMA system. Specifically, we derived the PDF of the e2e fading channel, which is then utilized to obtain an accurate PEP expression of NOMA users. As special cases, we derived novel PEP expressions for a single and large number of REs, where for the latter we adopted the CLT to obtain an alternative PDF for the e2e fading channel. The derived PEP expression was then exploited to evaluate a tight union bound on the BER. Furthermore, we evaluated the asymptotic PEP of the lth user, which was then used to quantify the asymptotic diversity order. The derived analytical results of the considered scenario, validated by Monte Carlo simulations, showed that the asymptotic diversity order of LIS-based NOMA systems depends on the number of REs (M). Finally, the obtained results highlighted the advantages of utilizing LIS to improve the diversity order of NOMA users, compared to

the conventional amplify-and-forward relaying, which limits the asymptotic diversity order of NOMA users to unity [3].

APPENDIX

In this Appendix, we provide the proof of Proposition 1 and derive the first four moments required for the derivation of the PDF of q_l.

A. Derivation of the Approximate PDF $f_{q_l}(q)$

By recalling that both $|h_m|$ and $|g_{m,l}|$ $\forall m = 1, \ldots, M$ are independent and identically Rayleigh distributed with zero mean and variance $2\sigma^2$, the PDF of $\beta_m^{(l)} = |h_m||g_{m,l}|$, which follows the double Rayleigh distribution, is given as the follows [43]:

$$f_{\beta_m^{(l)}}(b) = \frac{b}{\sigma^4} K_0\left(\frac{b}{\sigma^2}\right), \quad b > 0. \tag{47}$$

By exploiting [52, eq. (03.04.26.0008.01)], the PDF of $\beta_m^{(l)}$ can be rewritten as

$$\begin{aligned} f_{\beta_m^{(l)}}(b) &= \frac{b}{2\sigma^4} G_{0,2}^{2,0}\left(\frac{b^2}{4\sigma^4}\middle| \begin{matrix} -;- \\ 0,0;- \end{matrix}\right) \\ &= \frac{b}{2\sigma^4}\frac{1}{2\pi j}\int_{\mathcal{C}}\left(\frac{b^2}{4\sigma^4}\right)^{-s}\Gamma^2(s)ds \\ &= \frac{1}{\sigma^2}\frac{1}{2\pi j}\int_{\mathcal{C}}\left(\frac{b}{2\sigma^2}\right)^{-2s+1}\Gamma^2(s)ds \end{aligned} \tag{48}$$

where $\mathcal{C}$ is an appropriate complex contour ensuring the convergence of the above Mellin–Barnes integral (e.g., $[1/2 - j\infty, 1/2 + j\infty]$), and $j = \sqrt{-1}$. Using the change of variable approach, $t = 2s - 1$, one can see

$$\begin{aligned} f_{\beta_m^{(l)}}(b) &= \frac{1}{2\sigma^2}\frac{1}{2\pi j}\int_{\mathcal{C}}\left(\frac{b}{2\sigma^2}\right)^{-t}\Gamma^2\left(\frac{t+1}{2}\right)dt \\ &= \frac{1}{2\sigma^2}H_{0,2}^{2,0}\left(\frac{b}{2\sigma^2}\middle| \begin{matrix} -;- \\ \left(\frac{1}{2},\frac{1}{2}\right),\left(\frac{1}{2},\frac{1}{2}\right);- \end{matrix}\right) \end{aligned} \tag{49}$$

where $H_{p,q}^{m,n}(.\mid.)$ denotes Fox's H-function [53]. By recalling that the summation of M H-distributions can be tightly approximated by an H-distribution [54], the PDF of $q_l = \sum_{m=1}^{M}\beta_m^{(l)}$ can be accurately approximated by a Fox's H-function, relying on the moment-based density approximants method [54]. The resultant Fox's H-function can be represented as Meijer's G-function, as depicted in Proposition 1. The tightness of the approximation relies on the number of considered moments. In this work, we use the first four moments, (i.e., $i = 1, 2, 3, 4$), which provides a linear system with four equations and four unknown variables ($\mu_i, i \leq 4$). In the following, we provide detailed steps for the derivation of these moments.

B. Moments Derivation, μ_i, for $1 \leq i \leq 4$

To obtain the moments of q_l, we initially derive the first four moments of $\beta_m^{(l)}$, for $1 \leq m \leq 4$, as follows:

$$\begin{aligned} \mu_1^{(m)} &= \mathbb{E}\left[|h_m|\middle|g_{m,l}|\right] \\ &= \left(\sigma\sqrt{\frac{\pi}{2}}\right)^2 = \frac{\pi}{2}\sigma^2 \end{aligned} \tag{50}$$

$$\begin{aligned} \mu_2^{(m)} &= \mathbb{E}\left[|h_m|^2\middle|g_{m,l}\right|^2\Big] \\ &= \left(2\sigma^2\right)^2 = 4\sigma^4 \end{aligned} \tag{51}$$

$$\begin{aligned} \mu_3^{(m)} &= \mathbb{E}\left[|h_m|^3\middle|g_{m,l}\right|^3\Big] \\ &= \left(3\sigma^3\sqrt{\frac{\pi}{2}}\right)^2 = \frac{9\pi\sigma^6}{2} \end{aligned} \tag{52}$$

and

$$\begin{aligned} \mu_4^{(m)} &= \mathbb{E}\left[|h_m|^4\middle|g_{m,l}\right|^4\Big] \\ &= \left(8\sigma^4\right)^2 = 64\sigma^8. \end{aligned} \tag{53}$$

Using (50)–(53) and employing the multinomial theorem, the first four moments of q_l can be evaluated as

$$\mu_1 = \sum_{m=1}^{M}\mu_1^{(m)} = \frac{M\pi\sigma^2}{2} \tag{54}$$

and

$$\begin{aligned} \mu_2 &= \mathbb{E}\left[\left(\sum_{m=1}^{M}\beta_m^{(l)}\right)^2\right] \\ &= \underbrace{\sum_{m=1}^{M}\mathbb{E}\left[(\beta_m^{(l)})^2\right]}_{4M\sigma^4} + 2\sum_{m=1}^{M-1}\sum_{j=m+1}^{M}\underbrace{\mathbb{E}\left[\beta_m^{(l)}\right]\mathbb{E}\left[\beta_j^{(l)}\right]}_{(\frac{\pi}{2}\sigma^2)^2} \\ &= 4M\sigma^4 + M(M-1)\sigma^4\frac{\pi^2}{4}. \end{aligned} \tag{55}$$

Also, μ_3 and μ_4 are provided in (56), shown at the bottom of the previous page, and (57), shown at the top of

$$\mu_3 = \mathbb{E}\left[\left(\sum_{i=1}^{M}\beta_i^{(l)}\right)^3\right] = \begin{cases} \underbrace{\sum_{i=1}^{M}\mathbb{E}\left[(\beta_i^{(l)})^3\right]}_{\frac{9\pi M\sigma^6}{2}} + \underbrace{3\sum_{i=1}^{M}\sum_{\substack{\ell=1\\ \ell\neq i}}^{M}}_{M(M-1)}\underbrace{\mathbb{E}\left[\beta_i^{(l)}\right]\mathbb{E}\left[(\beta_\ell^{(l)})^2\right]}_{\frac{\pi}{2}\sigma^2\times 4\sigma^4} + \underbrace{6\sum_{i=1}^{M-2}\sum_{\ell=i+1}^{M-1}\sum_{k=\ell+1}^{M}}_{\binom{M}{3}}\underbrace{\mathbb{E}\left[\beta_i^{(l)}\right]\mathbb{E}\left[\beta_\ell^{(l)}\right]\mathbb{E}\left[\beta_k^{(l)}\right]}_{(\frac{\pi}{2}\sigma^2)^3} & \\ \qquad 6\pi M(M-1)\sigma^6 \qquad\qquad\qquad\qquad M(M-1)(M-2)\left(\frac{\pi}{2}x\right)^3\sigma^6 & M \geq 3 \\ 9\pi\sigma^6 + 3\times 2\times\frac{\pi}{2}\sigma^2\times 4\sigma^4 = 21\pi\sigma^6, & M = 2 \\ \frac{9\pi\sigma^6}{2}, & M = 1 \end{cases} \tag{56}$$

$$\mu_4 = \mathbb{E}\left[\left(\sum_{i=1}^{M}\beta_i^{(l)}\right)^4\right] = \begin{cases} \underbrace{\sum_{i=1}^{M}\mathbb{E}\left[(\beta_i^{(l)})^4\right]}_{64M\sigma^8} + \underbrace{6\sum_{i=1}^{M-1}\sum_{j=i+1}^{M}\mathbb{E}\left[(\beta_i^{(l)})^2(\beta_j^{(l)})^2\right]}_{6\times\binom{M}{2}\times(4\sigma^4)^2} + \underbrace{4\sum_{i=1}^{M}\sum_{\substack{j=1\\ j\neq i}}^{M}\mathbb{E}\left[(\beta_i^{(l)})^3\beta_j^{(l)}\right]}_{4\times M\times(M-1)\times\left(\frac{\pi}{2}\sigma^2\right)\times\frac{9\pi\sigma^6}{2}} \\ \quad + \underbrace{12\sum_{i=1}^{M}\sum_{\substack{j=1\\ j\neq i}}^{M}\sum_{\substack{k>j\\ k\neq i}}^{M}\mathbb{E}\left[(\beta_i^{(l)})^2\beta_j^{(l)}\beta_k^{(l)}\right]}_{12M\times\frac{(M-1)(M-2)}{2}\left(\frac{\pi}{2}\sigma^2\right)^2\times 4\sigma^4} + \underbrace{24\sum_{i<j<k<p}\mathbb{E}\left[\beta_i^{(l)}\beta_j^{(l)}\beta_k^{(l)}\beta_p^{(l)}\right]}_{24\times\binom{M}{4}\times\left(\frac{\pi}{2}\sigma^2\right)^4}, & M\geq 4 \\ 3\times 64\sigma^8 + \underbrace{6\sum_{i=1}^{2}\sum_{j=i+1}^{3}\mathbb{E}\left[(\beta_i^{(l)})^2(\beta_j^{(l)})^2\right]}_{6\times 3\times(4\sigma^4)^2} + \underbrace{4\sum_{i=1}^{3}\sum_{\substack{j=1\\ j\neq i}}^{3}\mathbb{E}\left[(\beta_i^{(l)})^3\beta_j^{(l)}\right]}_{4\times 6\times\frac{\pi}{2}\sigma^2\times\frac{9\pi\sigma^6}{2}} \\ \quad + \underbrace{12\left(\mathbb{E}\left[(\beta_1^{(l)})^2\beta_2^{(l)}\beta_3^{(l)}\right] + \mathbb{E}\left[(\beta_2^{(l)})^2\beta_1^{(l)}\beta_3^{(l)}\right] + \mathbb{E}\left[(\beta_3^{(l)})^2\beta_1^{(l)}\beta_2^{(l)}\right]\right)}_{12\times 3\times\left(\frac{\pi}{2}\sigma^2\right)^2\times 4\sigma^4}, & M=3 \\ 2\times 64\sigma^8 + \underbrace{4\left(\mathbb{E}\left[\beta_1^{(l)}\right]\mathbb{E}\left[(\beta_2^{(l)})^3\right] + \mathbb{E}\left[\beta_2^{(l)}\right]\mathbb{E}\left[(\beta_1^{(l)})^3\right]\right)}_{4\times 2\times\frac{\pi}{2}\sigma^2\times\frac{9\pi\sigma^6}{2}} + \underbrace{6\mathbb{E}\left[(\beta_1^{(l)})^2\right]\mathbb{E}\left[(\beta_2^{(l)})^2\right]}_{6\times(4\sigma^4)^2}, & M=2 \\ 64\sigma^8, & M=1 \end{cases} \tag{57}$$

the page, respectively. By performing some algebraic operations, (55)–(57) can be reduced as in (23)–(25), respectively. This concludes the proof of Proposition 1.

REFERENCES

[1] M. Giordani, M. Polese, M. Mezzavilla, S. Rangan, and M. Zorzi, "Toward 6G networks: Use cases and technologies," *IEEE Commun. Mag.*, vol. 58, no. 3, pp. 55–61, Mar. 2020.

[2] L. Bariah, S. Muhaidat, and A. Al-Dweik, "Error probability analysis of non-orthogonal multiple access over Nakagami- *m* fading channels," *IEEE Trans. Commun.*, vol. 67, no. 2, pp. 1586–1599, Feb. 2019.

[3] L. Bariah, S. Muhaidat, and A. Al-Dweik, "Error performance of NOMA-based cognitive radio networks with partial relay selection and interference power constraints," *IEEE Trans. Commun.*, vol. 68, no. 2, pp. 765–777, Feb. 2020.

[4] L. Dai, B. Wang, Z. Ding, Z. Wang, S. Chen, and L. Hanzo, "A survey of non-orthogonal multiple access for 5G," *IEEE Commun. Surveys Tuts.*, vol. 20, no. 3, pp. 2294–2323, 3rd Quart., 2018.

[5] S. M. R. Islam, N. Avazov, O. A. Dobre, and K.-S. Kwak, "Power-domain non-orthogonal multiple access (NOMA) in 5G systems: Potentials and challenges," *IEEE Commun. Surveys Tuts.*, vol. 19, no. 2, pp. 721–742, 2nd Quart., 2017.

[6] L. Bariah, S. Muhaidat, and A. Al-Dweik, "Error probability analysis of NOMA-based relay networks with SWIPT," *IEEE Commun. Lett.*, vol. 23, no. 7, pp. 1223–1226, Jul. 2019.

[7] M. Vaezi, R. Schober, Z. Ding, and H. V. Poor, "Non-orthogonal multiple access: Common myths and critical questions," *IEEE Wireless Commun.*, vol. 26, no. 5, pp. 174–180, Oct. 2019.

[8] L. Dai, B. Wang, Y. Yuan, S. Han, I. Chih-Lin, and Z. Wang, "Non-orthogonal multiple access for 5G: solutions, challenges, opportunities, and future research trends," *IEEE Commun. Mag.*, vol. 53, no. 9, pp. 74–81, Sep. 2015.

[9] A. S. de Sena *et al.*, "What role do intelligent reflecting surfaces play in non-orthogonal multiple access?" Feb. 2020. [Online]. Available: techrxiv.11791050.v1.

[10] E. Basar, M. D. Renzo, J. De Rosny, M. Debbah, M.-S. Alouini, and R. Zhang, "Wireless communications through reconfigurable intelligent surfaces," *IEEE Access*, vol. 7, pp. 116753–116773, 2019.

[11] L. Bariah *et al.*, "A prospective look: Key enabling technologies, applications and open research topics in 6G networks," Apr. 2020. [Online]. Available: https://arxiv.org/abs/2004.06049

[12] C. Liaskos, S. Nie, A. Tsioliaridou, A. Pitsillides, S. Ioannidis, and I. Akyildiz, "Realizing wireless communication through software-defined hypersurface environments," in *Proc. IEEE 19th Int. Symp. World Wireless Mobile Multimedia Netw. (WoWMoM)*, Jun. 2018, pp. 14–15.

[13] O. Yurduseven, S. D. Assimonis, and M. Matthaiou, "Intelligent reflecting surfaces with spatial modulation: An electromagnetic perspective," *IEEE Open J. Commun. Society*, vol. 1, pp. 1256–1266, 2020.

[14] J. Yuan, H. Q. Ngo, and M. Matthaiou, "Towards large intelligent surface (LIS)-based communications," *IEEE Trans. Commun.*, vol. 68, no. 10, pp. 6568–6582, Oct. 2020.

[15] J. Zhang, E. Björnson, M. Matthaiou, D. W. K. Ng, H. Yang, and D. J. Love, "Prospective multiple antenna technologies for beyond 5G," *IEEE J. Sel. Areas Commun.*, vol. 38, no. 8, pp. 1637–1660, Aug. 2020.

[16] K. Ntontin *et al.*, "Reconfigurable intelligent surfaces vs. relaying: Differences, similarities, and performance comparison," 2019. [Online]. Available: arXiv:1908.08747.

[17] C. Huang, A. Zappone, G. C. Alexandropoulos, M. Debbah, and C. Yuen, "Reconfigurable intelligent surfaces for energy efficiency in wireless communication," *IEEE Trans. Wireless Commun.*, vol. 18, no. 8, pp. 4157–4170, Aug. 2019.

[18] C. Huang, G. C. Alexandropoulos, A. Zappone, M. Debbah, and C. Yuen, "Energy efficient multi-user MISO communication using low resolution large intelligent surfaces," in *Proc. IEEE Globecom Workshops (GC Wkshps)*, 2018, pp. 1–6.

[19] H. Zhang, B. Di, L. Song, and Z. Han, "Reconfigurable intelligent surfaces assisted communications with limited phase shifts: How many phase shifts are enough?" *IEEE Trans. Veh. Technol.*, vol. 69, no. 4, pp. 4498–4502, Apr. 2020.

[20] M. Jung, W. Saad, Y. Jang, G. Kong, and S. Choi, "Performance analysis of large intelligent surfaces (LISs): Asymptotic data rate and channel hardening effects," *IEEE Trans. Wireless Commun.*, vol. 19, no. 3, pp. 2052–2065, Mar. 2020.

[21] B. Zheng, Q. Wu, and R. Zhang, "Intelligent reflecting surface-assisted multiple access with user pairing: NOMA or OMA?" *IEEE Commun. Lett.*, vol. 24, no. 4, pp. 753–757, Apr. 2020.

[22] Z. Ding and H. V. Poor, "A simple design of IRS-NOMA transmission," *IEEE Commun. Lett.*, vol. 24, no. 5, pp. 1119–1123, May 2020.

[23] M. Fu, Y. Zhou, and Y. Shi, "Intelligent reflecting surface for downlink non-orthogonal multiple access networks," in *Proc. IEEE Globecom Workshops (GC Wkshps)*, Waikoloa, HI, USA, Mar. 2020, pp. 1–6.

[24] X. Mu, Y. Liu, L. Guo, J. Lin, and N. Al-Dhahir, "Exploiting intelligent reflecting surfaces in multi-antenna aided NOMA systems," Oct. 2019. [Online]. Available: https://arxiv.org/abs/1910.13636

[25] G. Yang, X. Xu, and Y.-C. Liang, "Intelligent reflecting surface assisted non-orthogonal multiple access," Jul. 2019. [Online]. Available: https://arxiv.org/abs/1907.03133

[26] M. Fu, Y. Zhou, and Y. Shi, "Reconfigurable intelligent surface empowered downlink non-orthogonal multiple access," Oct. 2019. [Online]. Available: https://arxiv.org/abs/1910.07361

[27] A. U. Makarfi, K. M. Rabie, O. Kaiwartya, O. S. Badarneh, X. Li, and R. Kharel, "Reconfigurable intelligent surface enabled IoT networks in generalized fading channels," in *Proc. IEEE Int. Conf. Commun. (ICC)*, Jul. 2020, pp. 1–6.

[28] P. Mursia, V. Sciancalepore, A. Garcia-Saavedra, L. Cottatellucci, X. Costa-Pérez, and D. Gesbert, "RISMA: Reconfigurable intelligent surfaces enabling beamforming for IoT massive access," *IEEE J. Sel. Areas Commun.*, early access, Aug. 24, 2020, doi: 10.1109/JSAC.2020.3018829.

[29] C. Pan *et al.*, "Intelligent reflecting surface aided MIMO broadcasting for simultaneous wireless information and power transfer," *IEEE J. Sel. Areas Commun.*, vol. 38, no. 8, pp. 1719–1734, Aug. 2020.

[30] Z. Ding, L. Dai, and H. V. Poor, "MIMO-NOMA design for small packet transmission in the Internet of Things," *IEEE Access*, vol. 4, pp. 1393–1405, 2016.

[31] M. Shirvanimoghaddam, M. Condoluci, M. Dohler, and S. J. Johnson, "On the fundamental limits of random non-orthogonal multiple access in cellular massive IoT," *IEEE J. Sel. Areas Commun.*, vol. 35, no. 10, pp. 2238–2252, Oct. 2017.

[32] Y. Li, M. Jiang, Q. Zhang, and J. Qin, "Joint beamforming design in multi-cluster MISO NOMA intelligent reflecting surface-aided downlink communication networks," Sep. 2019. [Online]. Available: https://arxiv.org/abs/1909.06972

[33] T. Hou, Y. Liu, Z. Song, X. Sun, and Y. Chen, "MIMO-NOMA networks relying on reconfigurable intelligent surface: A signal cancellation based design," Mar. 2020. [Online]. Available: https://arxiv.org/abs/2003.02117

[34] J. Zuo, Y. Liu, E. Basar, and O. A. Dobre, "Intelligent reflecting surface enhanced millimeter-wave NOMA systems," May 2020. [Online]. Available: https://arxiv.org/abs/2005.01562

[35] M. Zeng, X. Li, G. Li, W. Hao, and O. A. Dobre, "Sum rate maximization for IRS-assisted uplink NOMA," Apr. 2020. [Online]. Available: https://arxiv.org/abs/2004.10791

[36] T. Hou, Y. Liu, Z. Song, X. Sun, Y. Chen, and L. Hanzo, 'Reconfigurable intelligent surface aided NOMA networks," Dec. 2019. [Online]. Available: https://arxiv.org/abs/1912.10044

[37] X. Yue and Y. Liu, "Performance analysis of intelligent reflecting surface assisted NOMA networks," Feb. 2020. [Online]. Available: https://arxiv.org/abs/2002.09907

[38] V. C. Thirumavalavan and T. S. Jayaraman, "BER analysis of reconfigurable intelligent surface assisted downlink power domain NOMA," Feb. 2020. [Online]. Available: https://arxiv.org/abs/2002.09453

[39] W. Tang *et al.*, "Wireless communications with reconfigurable intelligent surface: Path loss modeling and experimental measurement," *IEEE Trans. Wireless Commun.*, vol. 20, no. 1, pp. 421–439, Jan. 2021.

[40] V. Tarokh, N. Seshadri, and A. R. Calderbank, "Space-time codes for high data rate wireless communication: Performance criterion and code construction," *IEEE Trans. Inf. Theory*, vol. 44, no. 2, pp. 744–765, Mar. 1998.

[41] I. Gradshteyn and I. Ryzhik, *Table of Integrals, Series, and Products*, A. Jeffrey and D. Zwillinger, Eds. Amsterdam, The Netherlands: Academic, 2007.

[42] A. P. Prudnikov, Y. A. Brychkov, and O. I. Marichev, *Integrals and Series, Volume 3: More Special Functions*. New York, NY, USA: Gordon Breach, 1986.

[43] J. Salo, H. M. El-Sallabi, and P. Vainikainen, "The distribution of the product of independent Rayleigh random variables," *IEEE Trans. Antennas Propag.*, vol. 54, no. 2, pp. 639–643, Feb. 2006.

[44] A. P. Prudnikov, Y. A. Brychkov, and O. I. Marichev, *Integrals and Series, Volume 2: Special Functions*. New York, NY, USA: CRC Press, 1986.

[45] M. K. Simon, *Probability Distributions Involving Gaussian Random Variables: A Handbook for Engineers and Scientists*. New York, NY, USA: Springer, 2006.

[46] C. Tellambura, "Evaluation of the exact union bound for trellis-coded modulations over fading channels," *IEEE Trans. Commun.*, vol. 44, no. 12, pp. 1693–1699, Dec. 1996.

[47] J. Proakis and M. Salehi, *Digital Communications*, 5th ed. Gosport, U.K.: Ashford Colour Press, 2014.

[48] I. S. Ansari, F. Yilmaz, and M.-S. Alouini, "Performance analysis of free-space optical links over Málaga ($\mathcal{M}$) turbulence channels with pointing errors," *IEEE Trans. Wireless Commun.*, vol. 15, no. 1, pp. 91–102, Jan. 2016.

[49] J. M. Meredith, "Study on downlink multiuser superposition transmission for LTE," 3GPP, Sophia Antipolis, France, Rep. TR 36.859, Mar. 2015.

[50] Z. Ding, R. Schober, and H. V. Poor, "A general MIMO framework for NOMA downlink and uplink transmission based on signal alignment," *IEEE Trans. Wireless Commun.*, vol. 15, no. 6, pp. 4438–4454, Jun. 2016.

[51] J. R. Hershey and P. A. Olsen, "Approximating the Kullback Leibler divergence between gaussian mixture models," in *Proc. IEEE Int. Conf. Acoust. Speech Signal Process. (ICASSP)*, vol. 4, 2007, pp. 317–320.

[52] Wolfram. *Modified Bessel Function of the Second Kind*. Accessed: Feb. 15, 2021. [Online]. Available: http://functions.wolfram.com/PDF/BesselK.pdf

[53] E. Weisstein. (2020). FoxH-function. [Online]. Available: mathworld.wolfram.com/FoxH-Function.html

[54] F. E. Bouanani and D. B. da Costa, "Accurate closed-form approximations for the sum of correlated Weibull random variables," *IEEE Wireless Commun. Lett.*, vol. 7, no. 4, pp. 498–501, Aug. 2018.

Lina Bariah (Member, IEEE) received the M.Sc. and Ph.D. degrees in communications engineering from Khalifa University, Abu Dhabi, UAE, in 2015 and 2018, respectively.

She was a Visiting Researcher with the Department of Systems and Computer Engineering, Carleton University, Ottawa, ON, Canada, in Summer 2019. She is currently a Postdoctoral Fellow with the KU Center for Cyber-Physical Systems, Khalifa University. Her research interests include advanced digital signal processing techniques for communications, channel estimation, cooperative communications, nonorthogonal multiple access, cognitive radios, reconfigurable intelligent surfaces, underwater wireless communications, and visible light communications.

Dr. Bariah was a member of the technical program committee of the numerous IEEE conferences, such as ICC and Globecom. She is currently an Area Editor for *Physical Communication* (Elsevier).

Sami Muhaidat (Senior Member, IEEE) received the Ph.D. degree in electrical and computer engineering from the University of Waterloo, Waterloo, ON, Canada, in 2006.

From 2007 to 2008, he was an NSERC Postdoctoral Fellow with the Department of Electrical and Computer Engineering, University of Toronto, Toronto, ON, Canada. From 2008 to 2012, he was an Assistant Professor with the School of Engineering Science, Simon Fraser University, Burnaby, BC, Canada. He is currently a Professor with Khalifa University, Abu Dhabi, UAE, and an Adjunct Professor with Carleton University, Ottawa, ON, Canada. His research interests focus on advanced digital signal processing techniques for wireless communications, RIS, 5G and beyond, MIMO, optical communications, IoT with emphasis on battery-free devices, and machine learning.

Prof. Muhaidat is currently an Area Editor of the IEEE TRANSACTIONS ON COMMUNICATIONS and a Lead Guest Editor of the IEEE OJ-COMS "Large-Scale Wireless Powered Networks With Backscatter Communications" special issue. He served as a Senior Editor and an Editor for the IEEE COMMUNICATIONS LETTERS, an Editor for the IEEE TRANSACTIONS ON COMMUNICATIONS, and an Associate Editor for the IEEE TRANSACTIONS ON VEHICULAR TECHNOLOGY.

Paschalis C. Sofotasios (Senior Member, IEEE) received the M.Eng. degree from Newcastle University, Newcastle upon Tyne, U.K., in 2004, the M.Sc. degree from the University of Surrey, U.K., in 2006, and the Ph.D. degree from the University of Leeds, Leeds, U.K., in 2011.

His M.Sc. studies were funded by a scholarship from U.K.-EPSRC and the Ph.D. studies were sponsored by U.K.-EPSRC and Pace plc. He held academic positions with the University of Leeds; the University of California at Los Angeles, Los Angeles, CA, USA; the Aristotle University of Thessaloniki, Thessaloniki, Greece; the Tampere University of Technology, Tampere, Finland; and Khalifa University, Abu Dhabi, UAE, where he is currently an Assistant Professor with the Department of Electrical and Computer Engineering. His research interests include digital and optical wireless communications and topics relating to mathematics and statistics.

Dr. Sofotasios received the Exemplary Reviewer Award from the IEEE COMMUNICATIONS LETTERS, in 2012 and the IEEE TRANSACTIONS ON COMMUNICATIONS, in 2015 and 2016, respectively. He was a co-recipient of the Best Paper Award from ICUFN, in 2013. He has served as an Associate Editor for the IEEE COMMUNICATIONS LETTERS. He currently serves as a Guest Editor for the IEEE OPEN JOURNAL OF THE COMMUNICATIONS SOCIETY and an Associate Editor for *Frontiers in Communications and Networks*. He is a member of the technical program committee for the numerous IEEE conferences.

Faissal El Bouanani (Senior Member, IEEE) was born in Nador, Morocco, in 1974. He received the M.S. and Ph.D. degrees in network and communication engineering from Mohammed V University-Souissi, Rabat, Morocco, in 2004 and 2009, respectively.

In 2009, he joined the National High School of IT/ENSIAS College of Engineering, Mohammed V University, Rabat, where he is currently an Associate Professor. He has served as a Faculty Member with the University of Moulay Ismail, Meknes, Morocco, from 1997 to 2009. He advised many Ph.D. and master's students with Mohammed V and Moulay Ismail Universities. His research efforts have culminated in more than 80 papers in a wide variety of international conferences and journals. His current research interests include performance analysis and design of wireless communication systems.

Dr. El Bouananiwas has also been involved as a TPC Member in various conferences and IEEE journals. He is also an Associate Editor of IEEE ACCESS and an Associate Editor of *Frontiers in Communications and Networks* journals. He is serving also as a Lead Guest Editor of Physical Layer Security special issue in *Frontiers in Communications and Networks* journals. His Ph.D. thesis was awarded the best one by Mohammed V University-Souissi in 2010. He served as the TPC Chair of the ICSDE conferences and the General Co-Chair of ACOSIS'16 and CommNet'18 conferences. He serves as the General Chair of the 2019–2021 CommNet conferences.

Octavia A. Dobre (Fellow, IEEE) received the Dipl.Ing. and Ph.D. degrees from the Polytechnic Institute of Bucharest, Bucharest, Romania, in 1991 and 2000, respectively.

From 2002 to 2005, she was with the New Jersey Institute of Technology, Newark, NJ, USA. In 2005, she joined Memorial University, St. John's, NL, Canada, where she is currently a Professor and a Research Chair. She was a Visiting Professor with the Massachusetts Institute of Technology, Cambridge, MA, USA, and the Université de Bretagne Occidentale, Brest, France. Her research interests encompass various wireless technologies, such as nonorthogonal multiple access and full duplex, optical and underwater communications, and machine learning for communications. She has (co-)authored over 300 refereed papers in the above areas.

Prof. Dobre received the Best Paper Awards at various conferences, including IEEE ICC, IEEE Globecom, IEEE WCNC, and IEEE PIMRC. She serves as the Editor-in-Chief (EiC) of the IEEE Open Journal of the Communications Society. She was the EiC of the IEEE COMMUNICATIONS LETTERS, and a senior editor, an editor, and a guest editor for various prestigious journals and magazines. She also served as the general chair, the technical program co-chair, the tutorial co-chair, and the technical co-chair of symposia at numerous conferences. She was a Royal Society Scholar, a Fulbright Scholar, and a Distinguished Lecturer of the IEEE Communications Society. She is a Fellow of the Engineering Institute of Canada.

Walaa Hamouda (Senior Member, IEEE) received the M.Sc. and Ph.D. degrees in electrical and computer engineering from Queen's University, Kingston, ON, Canada, in 1998 and 2002, respectively.

In July 2002, he joined the Department of Electrical and Computer Engineering, Concordia University, Montreal, QC, Canada, where he is currently an Associate Professor. Since June 2006, he has been a Research Chair of Communications and Networking with Concordia University. His current research interests include wireless networks, MIMO spacetimeprocessing, multiuser communications, crosslayer design, and source and channel coding.

Dr. Hamouda has received many awards, including the Best Paper Award (WNS) of the ICC 2009 at Dresden.